Optical signatures of valence-band mixing in positive trion recombination spectra of double quantum dots

W. J. Pasek, M. P. Nowak, and B. Szafran

AGH University of Science and Technology, Faculty of Physics and Applied Computer Science, al. Mickiewicza 30, 30-059 Kraków, Poland

(Received 13 June 2013; revised manuscript received 22 April 2014; published 6 June 2014)

We consider optical signatures of valence band mixing in positive trion and exciton complexes in vertically stacked InGaAs quantum dots. We use the configuration interaction method and an axially symmetric four-band Luttinger-Kohn Hamiltonian (KL) that allows for heavy-hole and light-hole band mixing due to spin-orbit interaction. A scalar effective hole mass model is also included for comparison. We found essential differences (i.e., different recombination patterns) between the KL and separated-bands model spectra. In the weak-coupling regime for KL model, we obtained a good agreement with experimentally observed X patterns in contrast to the scalar effective mass model.

DOI: 10.1103/PhysRevB.89.245303 PACS number(s): 73.21.La, 78.55.Cr, 78.67.Hc

I. INTRODUCTION

The external electric field applied along the axis of a pair of vertically coupled quantum dots [1–3] tunes the carrier localization within the system, segregates the electrons from holes and thus dissociates exciton and exciton complexes. Since the photoluminescence signal is observed from a single-pair of dots, i.e., a single artificial molecule [4–8], the optical experiments provide a rich set of precise data on the properties of the confined carriers and their interactions within the system [9–20].

In the last several years, there has been an increasing interest in the semiconductor nanostructures confining holes of the valence band, and the confined hole systems. The main motivation for this is the present state of knowledge in the field of spin interactions, which suggests that confined electron spins are ruled out as information carriers in III-V semiconductors due to coupling to the nuclear spin field and that the spins of holes are more promising candidates for this task [9,10]. The holes of the top of valence band occupy wave functions built of p-type atomic orbitals for which the Fermi contact interaction with nuclei vanishes, in contrast to electrons of the bottom of conduction band where wave functions are formed by s-type orbitals. Due to the degeneracy of the top of the valence band, the hole orbitals of the artificial molecules differ significantly from the electron ones. Namely, as a result of the valence band mixing, an antibonding hole ground state was found [11–14], a phenomenon that has no counterpart in natural molecules.

Usually, the hole systems in quantum dots are studied by means of capacitance voltage [15] and tunneling [16] spectroscopy. A positive trion is the simplest of exciton complexes that allows to study both hole-hole and electron-hole interactions in photoluminescence (PL) spectroscopy experiments in the few-eV energy range [17,18], with a precision of a fraction of μeV.

Charged complexes have been studied experimentally with photoluminescence spectroscopy (see Ref. [17–19]). In particular, for positive trions, characteristic X patterns were found in the experimental spectra. In Refs. [17,18], also the g factor of a positive trion near the X pattern was measured, as a mean for determination of the bonding/antibonding hole character. A PL experiment on positive trions in laterally coupled quantum dots was also conducted [20]. A full configuration interaction study of the spontaneous recombination of neutral and singly charged excitons (trions) in single semiconductor quantum dots was presented in Ref. [21]. Positive trions in quantum dot molecules were theoretically studied with a single-band effective mass model for holes and within the approximation of frozen lateral degrees of freedom [22].

In the present work, we investigate the consequences of valence band mixing in photoluminescence spectra of positive trions: whether it results in the formation of an antibonding hole ground state within the trion and, if so, what are the PL signatures of such a state. We employ a configuration interaction method and a scalar effective mass model for electrons. We use a four-band axially symmetric version of the Luttinger-Kohn hole Hamiltonian (KL) that allows for heavy-hole (HH) and light-hole (LH) band mixing as a result of spin-orbit interaction. The results are compared with an isotropic single-hole effective mass approximation. We demonstrate that in a strongly coupled asymmetric molecule as well as in symmetric systems, in the central part of the spectrum, there is a remarkable reversal of maximum/minimum recombination probability between the KL and separated-bands models. We explain that this is a direct consequence of the antibonding/bonding character of the two-hole ground state in the positive trion. We find that the trion dissociation pattern is completely different for both models for certain barrier thickness with respect to recombination energy shift and particle tunneling sequence. We obtained the energy redshift/blueshift reversal in the low dipole moment recombination lines and we discuss its role in the different dissociation pattern formation. The results are also compared to the ones obtained previously for negatively charged trions.

II. THEORY

We consider below both the exciton and the positive trion. We compare results obtained with four-band Kohn Luttinger [23] and separated-bands Hamiltonians with *isotropic* effective masses for heavy and light holes. We work in the effective mass approximation and envelope ansatz. We model the confinement potential of the pair of vertically stacked InGaAs quantum dots by a double rectangular quantum well along the z axis of heights 2.0 and 2.1 nm for the bottom and the top

dots, respectively. The depth of the well results from the band offset between the InGaAs dot and the GaAs matrix. Since all phenomena related to the interdot tunneling and exciton dissociation occur in the growth direction (z axis), for simplicity, we take an infinite quantum well for the confinement in the direction perpendicular to the growth direction. Moreover, the dots are assumed circularly symmetric, with radius $R = 10$ nm.

We use the following Hamiltonian for the exciton consisting of an electron in the conduction band and a hole in the valence band:

$$\hat{H}_{\text{exc}} = \hat{H}_e\mathbf{I} + \hat{H}_h + \hat{H}^{\text{int}}_{eh} + \hat{H}^{F}_{\text{exc}}, \tag{1}$$

where $\mathbf{I}$ is the identity matrix of the space (HH↑,LH↓,LH↑, HH↓) $= (|\frac{3}{2},+\frac{3}{2}\rangle,|\frac{3}{2},-\frac{1}{2}\rangle,|\frac{3}{2},+\frac{1}{2}\rangle,|\frac{3}{2},-\frac{3}{2}\rangle)$. For the positive trion formed by two holes and an electron, the operator

$$\hat{H}_{\text{trion}} = \hat{H}_{h1} + \hat{H}_{h2} + \hat{H}_e\mathbf{I} + \hat{H}^{\text{int}}_{e,h1} + \hat{H}^{\text{int}}_{e,h2} + \hat{H}^{\text{int}}_{h1,h2} + \hat{H}^{F}_{\text{trion}} \tag{2}$$

is used, where $\hat{H}_h$ represents the one-particle Hamiltonian for a hole ($\hat{H}_{h1}$ and $\hat{H}_{h2}$ "first" and "second" holes in the trion, respectively), $\hat{H}_e$ stands for the one-particle Hamiltonian of an electron, $\hat{H}^{\text{int}}_{\alpha\beta} = \pm\frac{1}{\epsilon r_{\alpha\beta}}\mathbf{I}$ is the Coulomb interaction for a pair of particles (α,β) (atomic units). $\hat{H}^{F}_{\text{exc}} = e(z_h - z_e)F\mathbf{I}$ and $\hat{H}^{F}_{\text{trion}} = e(z_{h1} + z_{h2} - z_e)F\mathbf{I}$ are the external electric field Hamiltonians as the field is externally applied along the z axis (F is the field strength) for the exciton and trion, respectively.

The kinetic energy of an electron in a nondegenerate conduction band is given by $\hat{T}_e = -\frac{1}{2m^*_e}\nabla^2_e$. The kinetic energy for the hole in the valence band is calculated using the axial approximation of the KL Hamiltonian [23] accounting for the light- and heavy-hole bands that are degenerate at the top of the valence band. The Hamiltonian written in the basis presented above has the following form:

$$\hat{T}_h = \hat{KL} = \begin{pmatrix} \hat{P}_+ & \hat{R} & -\hat{S} & 0 \\ \hat{R}^* & \hat{P}_- & 0 & \hat{S} \\ -\hat{S}^* & 0 & \hat{P}_- & \hat{R} \\ 0 & \hat{S}^* & \hat{R}^* & \hat{P}_+ \end{pmatrix}, \tag{3}$$

where $\hat{P}_+ = \frac{1}{2}[(\gamma_1+\gamma_2)\hat{p}^2_\perp + (\gamma_1 - 2\gamma_2)\hat{p}^2_z]$, $\hat{P}_- = \frac{1}{2}[(\gamma_1 - \gamma_2)\hat{p}^2_\perp + (\gamma_1 + 2\gamma_2)\hat{p}^2_z]$, $\hat{R} = -\frac{\sqrt{3}}{2}\frac{\gamma_2+\gamma_3}{2}\hat{p}^2_-$, $\hat{S} = \sqrt{3}\gamma_3\hat{p}_-\hat{p}_z$, $\hat{p}_- = \hat{p}_x - i\hat{p}_y$, and $\hat{p}_\perp = \hat{p}^2_x + \hat{p}^2_y$. $\gamma_1,\gamma_2,\gamma_3$ are Luttinger parameters.

The one-electron and one-hole-band eigenfunctions have the form

$$\Psi^{\text{el}}_j(\vec{r}_e) = \exp(il\phi)J_l\left(\frac{\kappa_{kl}\rho}{R}\right)Z_n(z), \tag{4}$$

where J_l is a Bessel function of the first kind and κ_{kl} is the kth zero of that function. The one-hole KL eigenfunctions are four-component spinors,

$$\Psi^{\text{ho}}_{j_h,l_h}(\vec{r}_h) = \begin{pmatrix} \xi^{\text{HH}\uparrow}_{j_h} e^{il_h\phi} \\ \xi^{\text{LH}\downarrow}_{j_h} e^{i(l_h+2)\phi} \\ \xi^{\text{LH}\uparrow}_{j_h} e^{i(l_h+1)\phi} \\ \xi^{\text{HH}\downarrow}_{j_h} e^{i(l_h+3)\phi} \end{pmatrix}, \tag{5}$$

for the state of the total angular momentum $(l_h + \frac{3}{2})\hbar$.

In the calculations, we assume a dielectric constant $\epsilon = 12.9$. All the other material parameters were taken from the work of Vurgaftman *et al.* [24] using nonzero bowing parameters when appropriate. In this paper, the degenerate top of GaAs valence band and the bottom of the GaAs conduction band are assumed as reference energy levels, for the hole and the electron, respectively. Therefore all the recombination energies given below are calculated with respect to GaAs band-gap energy.

The evaluation of the Coulomb matrix elements of exciton basis functions is done by translating the problem of six-dimensional integration to solving the Poisson equation with appropriate inhomogeneity [25] by the sequential overrelaxation method on meshes with multigrid strategy. At the beginning, the one-particle electron Hamiltonian eigenequation for electrons and one-band one-particle hole Hamiltonian eigenequations are solved. Separable parts of those wave functions in the growth direction [$Z_n(z)$ in Eq. (4)] are determined by a direct diagonalization on a one-dimensional mesh with mesh spacing $\Delta z = 0.1$ nm. Then the hole eigenfunctions are obtained in a basis constructed with $k \in \{1,2\}$, $n \in \{1,30\}$, and $l \in \{-6,3\}$. Next, the variational basis for the exciton and the trion is constructed.

The trion basis functions are constructed with hole function antisymmetrization

$$\begin{aligned}\Phi^{\text{trion}}_\zeta(\vec{r}_e,\vec{r}_{h1},\vec{r}_{h2}) &= \Phi^{\text{trion}}_{k_e,l_e,n_e,j_{h1},l_{h1},j_{h2},l_{h2}}(\vec{r}_e,\vec{r}_{h1},\vec{r}_{h2}) \\ &= \Psi^{\text{el}}_{k_e,l_e,n_e}(\vec{r}_e)\big[\Psi^{\text{ho}}_{j_{h1},l_{h1}}(\vec{r}_{h1})\Psi^{\text{ho}}_{j_{h2},l_{h2}}(\vec{r}_{h2}) \\ &\quad - \Psi^{\text{ho}}_{j_{h2},l_{h2}}(\vec{r}_{h1})\Psi^{\text{ho}}_{j_{h1},l_{h1}}(\vec{r}_{h2})\big]\end{aligned} \tag{6}$$

using KL (or separated-bands) eigenfunctions corresponding to the 36 lowest eigenenergies and electron one-particle eigenfunctions with $k_e = 1, l_e \in \{-2,2\}$ and $n_e \in \{1,2\}$, which gives the basis of 360 elements for the exciton and 6300 elements for the trion.

In this work, the radiative recombination probability of interband excitonic transitions is calculated using the envelope approximation to Fermi golden rule,

$$I = |\vec{\epsilon}\cdot\vec{p}_{\text{if}}|^2 = |\vec{\epsilon}\cdot\langle u_{v_{\text{in}}}|\vec{p}|u_{v_{\text{fi}}}\rangle\langle\chi_{\text{in}}|\chi_{\text{fi}}\rangle|^2. \tag{7}$$

In the foregoing formula, u_{fi} and u_{in} are *electron* Bloch functions of the final or initial state, respectively, and χ_{fi} and χ_{in} are *electron* envelope functions of the final or initial state, respectively. This procedure leads to final expressions for normalized oscillation strength for the exciton,

$$\begin{aligned} I &= \sum_{j\in\{\text{HH}\uparrow,\text{LH}\downarrow,\text{LH}\uparrow,\text{HH}\downarrow\}} \eta_j|I_j|^2, \\ I_j &= \sum_\zeta c^\zeta \iint d^3\vec{r}_h d^3\vec{r}_e \xi^j_{j_{h1}}(\vec{r}_h)e^{i(l_{h1}+a)\phi} \\ &\quad \times \Psi^{\text{el}}_{k_e,l_e,n_e}(\vec{r}_e)\delta(\vec{r}_h,\vec{r}_e), \end{aligned} \tag{8}$$

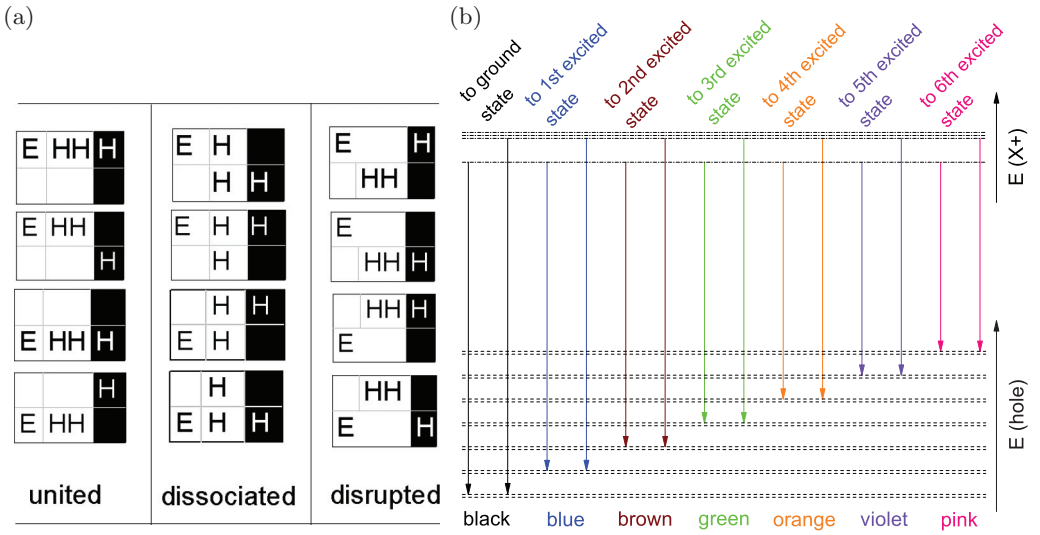

FIG. 1. (Color online) (a) Definition of terms *united*, *dissociated*, and *disrupted* that are used in the text for characterization of the trion initial states and recombination lines. (b) Color line sequence used in spectra figures. Dash-dotted lines denote the initial trion state (singlets or triplets), dash lines denote the final hole states.

and for the trion,

$$
\begin{aligned}
I &= \sum_{j\in\{\mathrm{HH}\uparrow,\mathrm{LH}\downarrow,\mathrm{LH}\uparrow,\mathrm{HH}\downarrow\}} \eta_j(|I_{j,1}|^2+|I_{j,2}|^2),\\
I_{j,1} &= \sum_{\zeta} c^{\zeta} \iiiint d^3\vec{r}_{h1}d^3\vec{r}_{h2}d^3\vec{r}_e d^3\vec{r}_{h\mathrm{fi}}\xi^{j}_{j_{h1}}(\vec{r}_{h1})\\
&\quad\times e^{i(l_{h1}+a)\phi}\Psi^{\mathrm{el}}_{j_e}(\vec{r}_e)\Psi^{\mathrm{ho}}_{j_{h2}}(\vec{r}_{h2})\Psi^{\mathrm{ho}}_{\mathrm{fi}}(\vec{r}_{h\mathrm{fi}})\\
&\quad\times\delta(\vec{r}_{h1},\vec{r}_e)\delta(\vec{r}_{h2},\vec{r}_{h\mathrm{fi}}),\\
I_{j,2} &= \sum_{\zeta} c^{\zeta} \iiiint d^3\vec{r}_{h1}d^3\vec{r}_{h2}d^3\vec{r}_e d^3\vec{r}_{h\mathrm{fi}}\xi^{j}_{j_{h2}}(\vec{r}_{h2})\\
&\quad\times e^{i(l_{h2}+a)\phi}\Psi^{\mathrm{el}}_{j_e}(\vec{r}_{e1})\Psi^{\mathrm{ho}}_{j_{h1}}(\vec{r}_{h1})\Psi^{\mathrm{ho}}_{\mathrm{fi}}(\vec{r}_{h\mathrm{fi}})\\
&\quad\times\delta(\vec{r}_{h2},\vec{r}_e)\delta(\vec{r}_{h1},\vec{r}_{h\mathrm{fi}}),
\end{aligned}
\tag{9}
$$

where [26] $\eta_{\mathrm{HH}\uparrow}=\eta_{\mathrm{HH}\uparrow}=1,\eta_{\mathrm{LH}\uparrow}=\eta_{\mathrm{LH}\uparrow}=\frac{1}{3}$, $a\in 0,2,1,3$ [see Eq. (5)], and h_{fi} refers to the final state of a hole that remains after the electron-hole recombination.

The actual intensities of the experimental spectra are affected by formation probability of the initial states that strongly depends on the way the sample is excited [27]. Moreover, in order to produce a PL signal the initial state needs to survive till the recombination. The excited states relax to the ground-state by emitting phonons and infrared radiation due to the intraband transitions. We simulate these effects by multiplying the recombination probabilities by a Boltzmann-like factor of $\exp(-\Delta E/E_r)$, where ΔE is the spacing between the initial and the ground states of the trion or exciton, and where we set $E_r = 34$ meV [28].

III. RESULTS

For a more specific characterization of the recombination lines, the particle localization diagrams were added to the figures presented in the following sections (Figs. 2, 5, 8). Only positive trion emission lines (and not neutral exciton lines) have been described in this way for transparency of the pictures. The mentioned diagrams are tables with two rows and three columns. The left column presents the localization of the electron in the initial trion state. The central column presents the localization of the hole in the initial trion state. The right column presents the localization of the final hole. The upper row is for the top dot and the lower one for the bottom dot. The localizations were determined by calculating the charge density of the relevant particle. The majuscule denotes a whole or a dominant part of the charge density. The minuscule denotes a minority of the charge density. The asterisk denotes a radial in-plane excitation visible in the particle density.

The red lines correspond to the neutral exciton recombination. All the other colors mark the positive trion recombination to different final hole states. Black lines indicate recombination to the ground state of the hole, blue lines to the first excited state, and the sequence continues in the following order: brown, green, orange, violet, and pink. The terms united, dissociated, disrupted (used for description of particle location), and the color line sequence are illustrated in Fig. 1 [29].

Energy spectra obtained for an asymmetrical dot pair are presented on Figs. 2, 5, and 8 for barrier thicknesses D equal 4.1, 7.1, and 10.1 nm, respectively. The recombination probability is presented as the size of data points (and hence as the thickness of lines).

A. Asymmetric dots, strong coupling: double maximum

The overall type of the energy spectra in Fig. 2 is quite similar for KL (a) and for separated-bands (b) Hamiltonians. Generally, the KL Hamiltonian leads to slightly lower energies of the whole spectrum. The "ground" recombination line of the trion (i.e., recombination line from the ground initial state of the trion to the ground initial state of the hole) originates from a singlet state. It has two maxima, one for a negative and one for a positive value of F_z with a single minimum in between. This structure is an effect of interplay between the change in the energy of the initial state and the energy of the

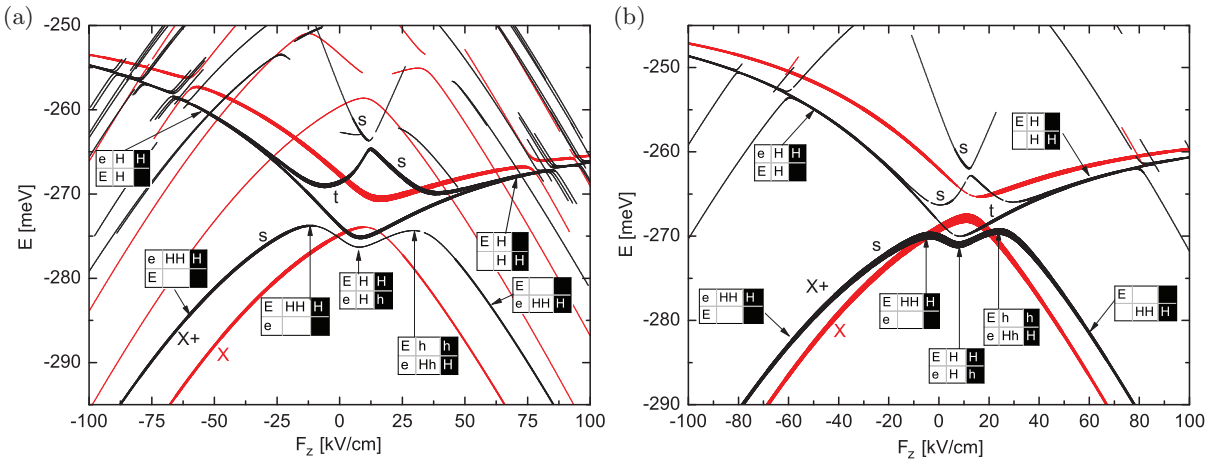

FIG. 2. (Color online) Energy spectrum and recombination probabilities (marked as line width) for positive trion and exciton vs electric field intensity parallel to z axis. The case of asymmetric dots with barrier width $D = 4.1$ nm: (a) for the KL Hamiltonian and (b) for the unmixed HH and LH bands Hamiltonian. Red color indicates the exciton recombination probability and black is for the trion recombination to hole ground state. Particle localization diagrams are described in the text. A letter "s" denotes a singlet initial state, "t" denotes a triplet state.

final hole state. The central minimum corresponds to a roughly even distribution of particle densities between the dots.

To investigate the origin of double maximum, we calculated (i) the energy difference between the *singlet* ground initial trion state and the first excited *singlet* initial state and (ii) the energy difference between the ground final hole state and the first excited final hole state. Both energy levels are shown in Fig. 3. If every particle is located entirely in one of the dots then the level has an approximately constant dipole moment. Also the energy difference of such two levels has approximately constant dipole moment and hence it is nearly linear as the function of F_z. We identify minima of the initial states energy difference (green line) as a hole

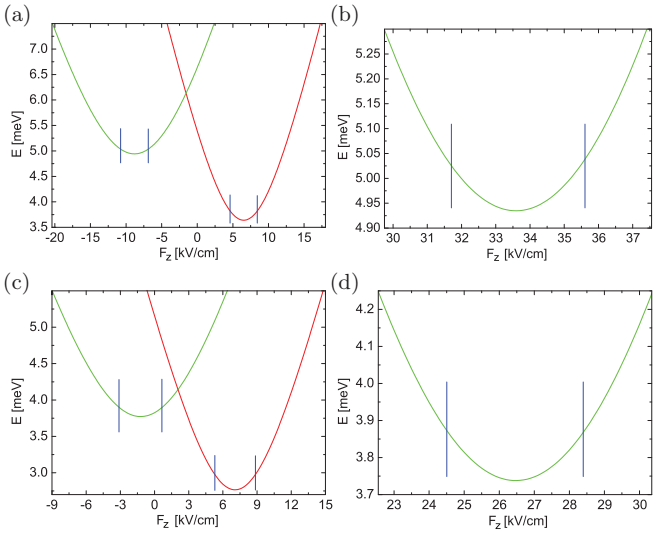

FIG. 3. (Color online) Energy difference between two lowest-energy singlet states (green line) and between two lowest-energy nondegenerated hole final states (red line) for an asymmetric system, 4.1 nm barrier. Each blue line marks a tunneling interval of the corresponding particle. (a) and (b) For the KL Hamiltonian. (c) and (d) For the unmixed HH and LH band Hamiltonians. See text for details.

tunneling in the trion state. We also identify the minimum of the final states energy difference (red line) as a hole tunneling in the final state. We have also determined tunneling intervals for each particle (ends marked with blue vertical lines) [30]. The resulting tunneling intervals have been marked on relevant fragments of the respective spectra (Fig. 4). It can be noticed that maxima in transition energy between the initial trion ground state and the final hole ground state (ground-ground) correspond approximately to the tunneling of initial state holes [$F_z \in (-10.8, -6.9)$ kV/cm and $F_z \in (4.6,8.4)$ kV/cm for KL model; $F_z \in (-3.1,0.7)$ kV/cm and $F_z \in (5.3,8.9)$ kV/cm for separated-bands model] and central minimum corresponds approximately to the final hole tunneling [$F_z \in (31.7,35.6)$ kV/cm for the KL model; $F_z \in (24.5,28.4)$ kV/cm for the separated-bands model]. Moreover, the sequence of the tunneling processes is identical for the KL and the separated-bands results. The tunneling processes are separate in both cases.

B. Asymmetric dots, strong coupling: strong F_z limits

With the increase of the absolute value of F_z, the ground line eventually decreases both in the energy and in the recombination probability. This is a sign of a complete disruption of the initial trion [by *disruption* we mean that the electron is localized in one of the dots and both holes are localized in the other one, see Fig. 1(a)]. It should be noted that for strong coupling the process of trion dissociation as a function of the applied external field proceeds continuously over a relatively large interval of F_z. In this regime, particles are not unambiguously localized in one of the dots (especially the electron).

For strong F_z, we also find bright levels that tend to stabilize their energy. These lines acquire the energies of approximately -255 meV for $F_z = -100$ kV/cm and -265 meV for $F_z = +100$ kV/cm in the case of the KL and -250 meV for $F_z = -100$ kV/cm and -260 meV for $F_z = +100$ kV/cm in the separated-bands case [Figs. 2(a) and 2(b), respectively]. The discussed levels correspond to the *dissociated* [see Fig. 1(a)]

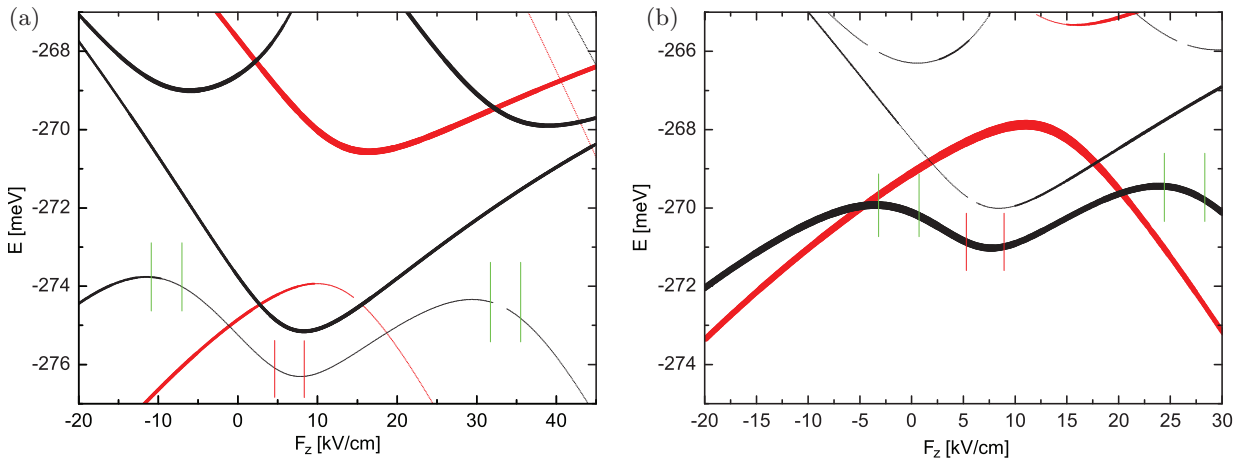

FIG. 4. (Color online) Fragments of the corresponding spectra from Fig. 2 with tunneling intervals from Fig. 3 marked by vertical lines: green for trion initial state hole, red for final state hole.

positive trion, with their dipole moments approaching zero in the very strong electric field. These levels are in fact the strong field limits for four distinct states: a triplet-originating level that approaches the given limit from "below" and a singlet-originating level that is coming from above (and from this point they will be referred to as *limit levels*). The energies of these lines approach the corresponding single dot neutral exciton line. This is because the dissociated trion is effectively decomposed to the exciton state and the second hole in the other dot. The difference in the energy between the trion and exciton states comes from the residual interdot Coulomb interaction.

C. Asymmetric dots, strong coupling: bonding/antibonding character

Let us compare the separated-bands model results with the KL model results. The first slight difference between results obtained for both Hamiltonians can be found in *dissociated* levels: the KL Hamiltonian yields many more hole anticrossings of small energy in that section of the spectrum than the separated-bands Hamiltonian. This is a consequence of the fact that KL permits formation and mixing of the states that would be completely unmixed when the bands are separated. The space spanned by the eigenstates of the KL Hamiltonian is therefore much bigger. The most significant difference between the spectra is the reversal of the maximum and the minimum of recombination probability within the central part of the spectrum between the lowest lying singlet level (the black "ground" recombination line) and the lowest lying triplet state (the black "first excited" level, i.e., recombination from one of the triple degenerated first excited trion states to a final hole ground state). In the KL model, the ground level has a *minimum* of the recombination probability in the vicinity of $F_z = 0$ and the first excited level has *maximal* recombination probability in the same region. In the separated bands, the pattern is reversed. This is a direct result of the light and heavy-hole band mixing, leading to the formation of an "antibonding" hole ground state [11–14].

The heavy-hole ground state is always bonding in character for $F_z = 0$ (in particular, it has even parity for a symmetric dot system) and so is the light-hole ground state in the single-band model. However, the KL Hamiltonian mixes the bands in such a way that its eigenstates have leading heavy-hole and leading light-hole components of opposing "bonding/antibonding character" (i.e., bonding HH and antibonding LH components and vice versa). As the low-lying KL eigenstates have a heavy-hole contribution much larger than their light-hole contribution, the bonding character of the whole KL eigenstate is determined as the bonding character of the dominating HH component of that state [31].

In the central point of the spectra Figs. 2(a) and 2(b) ($F_z < 25$ kV/cm), the particle density scheme is nearly the same for the ground level and for the first excited level (for clarity purposes, only the diagram for the ground level has been placed in the picture). In conclusion, the particle localization can not be responsible for the variation of probability mentioned above. To describe the process of maximal/minimal recombination probability reversal, we have studied the bonding character of the hole part of the trion, the electron part of the trion and final hole state for both Hamiltonians. The electron part of the trion state in the low-energy states was assumed bonding, as a free electron is described by a scalar effective mass and thus it has a bonding ground state (similar to the separated hole band) and the small value of this mass makes the excitation energy high. The final hole bonding/antibonding character was determined by calculating the expected value of parity along the z axis:

$$\langle Pz\rangle_h^{\text{fin}} = \int \Psi^*_{\text{fin}}(\phi,\rho,z)\Psi_{\text{fin}}(\phi,\rho,-z)d^3\vec{r}_{\text{fin}}, \tag{10}$$

and the bonding/antibonding character of the hole part of the trion state was determined by calculating the *normalized* expected value of parity along the z axis:

$$\begin{aligned} f(\vec{r}_e,\vec{r}_{h1},\vec{r}_{h2}) &= \Omega^*_{\text{trion}}(\vec{r}_e,\phi_{h1},\rho_{h1},z_{h1},\vec{r}_{h2}) \\ &\quad\times\Omega_{\text{trion}}(\vec{r}_e,\phi_{h1},\rho_{h1},-z_{h1},\vec{r}_{h2}), \\ \langle Pz\rangle_h^{\text{trion}} &= \frac{\int f(\vec{r}_e,\vec{r}_{h1},\vec{r}_{h2})d^3\vec{r}_e d^3\vec{r}_{h1}d^3\vec{r}_{h2}}{\int |f(\vec{r}_e,\vec{r}_{h1},\vec{r}_{h2})|d^3\vec{r}_e d^3\vec{r}_{h1}d^3\vec{r}_{h2}}, \end{aligned} \tag{11}$$

where $\Psi_{\text{fin}}(\vec{r}_{\text{fin}})$ and $\Omega_{\text{trion}}(\vec{r}_e,\vec{r}_{h1},\vec{r}_{h2})$ are the relevant final hole and trion wave functions, respectively.

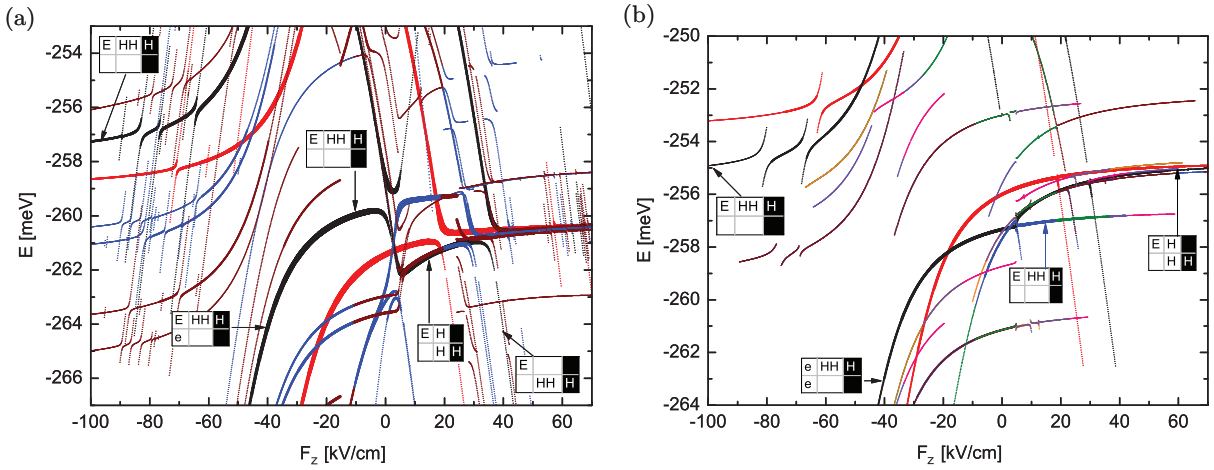

FIG. 5. (Color online) Same as Fig. 2 only for interdot barrier of 7.1 nm. Blue color is for trion recombination to a hole first excited state and the other colors are for successive excited final hole states.

For the separated-bands Hamiltonian [Fig. 4(b)], the central energy minimum for the ground level occurs for $F_z = 7.7$ kV/cm and for the first excited level, for $F_z = 8.4$ kV/cm. The calculated expected values of a final hole parity in that point equals to 0.22 and 0.15, respectively, so it is bonding [31]. The calculated normalized parity values of the trion hole part in these points are equal to 0.44 and 0, respectively, so both holes in the trion ground state are bonding while one is bonding and one is antibonding in the first excited one. Therefore we can write "bonding character description" in the form of $(\langle Pz\rangle_e^{\text{trion}}, (\langle Pz\rangle_{h_1}^{\text{trion}}, \langle Pz\rangle_{h_2}^{\text{trion}}), \langle Pz\rangle_{h_{\text{fin}}}^{\text{fin}})$ (marking + for the bonding character and - for the antibonding character) for the ground level recombination, (+,(+,+),+), and for the first excited level, (+,(+,−),+). The formula for the recombination probability depends on the overlap of electron and hole parts, and also on the overlap value of the hole part and final hole state. If the particles are distributed more or less equally between the dots (as in the central region of the spectrum), then the overlap between the states of opposite bonding character is more or less equal to zero. In the ground level transition (+,(+,+),+), all particles occupy bonding orbitals and the mentioned situation does not occur. However, in the excited level transition (+,(+,−),+), either the electron bonding orbital does not match the hole antibonding orbital or the bonding final hole state does not match the hole antibonding orbital. In consequence, the recombination probability vanishes in the first excited level but not in the ground level.

For the KL Hamiltonian [Fig. 4(a)], the central energy minimum occurs for $F_z = 7.9$ kV/cm and for the first excited level, for $F_z = 8.3$ kV/cm. The expected values of final hole parity in those points equals −0.28 and −0.25, respectively, so the hole in the final state occupies an antibonding orbital. The normalized parity values of the trion hole part in the mentioned points are equal to −0.35 and 0.03, respectively, so both holes in the trion ground state are antibonding, while one is bonding and one is antibonding in the first excited one. The "bonding character description" for the ground level recombination is (+,(−,−),−) and for the first excited level, (+,(+,−),−). In the transition from the first excited level, the electron of the bonding orbital recombines with the hole of the bonding orbital. Then the final state of the hole is the antibonding ground state and matches the remaining hole from the trion initial state. On the other hand, the recombination from the ground state is forbidden since both holes occupy antibonding orbitals and do not match the symmetry of the electron bonding orbital. In consequence, the recombination probability vanishes in the ground level but not in the first excited level.

D. Asymmetric dots, the case of medium coupling

The central part of both the KL [Fig. 5(a)] and separated-band [Fig. 5(b)] spectra for barrier thickness 7.1 nm contain a series of large anticrossings due to the interdot electron tunneling [32]. However, unlike the previous case, a remarkable difference between the results in the shape of the spectrum is also visible. The dissociated trion *limit levels* (described above for 4.1 nm barrier) appear also in this system. They are represented by the black line, and are accompanied with lines in other colors with similar energy behavior. Other colors represent recombination to the successive excited states of the final hole. The mentioned "color" levels mark the transition from the dissociated trion states in which the excitonlike part (i.e., electron and the hole parts of the trion function localized in the same dot) is very similar to the relevant parts of the trion state in the "black" dissociated level and the "odd" hole part is very similar to the relevant excited final hole state (levels of that kind have been illustrated with diagrams for the barrier 10.1 nm, below). Therefore the argument for energy convergence holds also in the case of the "color" levels.

For a barrier thickness of 7.1 nm, another interesting level can be seen that is a result of recombination from a *united* trion state (i.e., the trion state in which all particle parts are localized in a single dot, see Fig. 1). The *united limit levels* have energy circa −257 meV (black line) for $F_z = -100$ and −259 meV (blue and then brown line, discontinued) for $F_z = 20$ kV/cm in the KL results [Fig. 5(a)]; −255 meV for $F_z = -100$ kV/cm (black line), and −257 meV for $F_z = 60$ kV/cm (pink line, discontinued). It should be noticed that while in Fig. 5(a) the high field energy limit lies over the exciton line (is blueshifted), in Fig. 5(b), the limit lies under the exciton

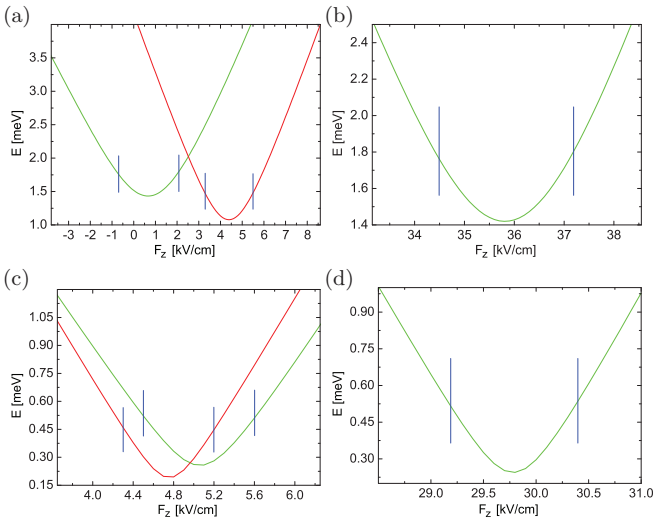

FIG. 6. (Color online) Same as Fig. 3 only for interdot barrier of 7.1 nm.

energy (is redshifted). The key difference between the spectra in Figs. 5(a) and 5(b) (described in the next paragraph) is a consequence of the shift type reversal. This observation is one of the main results of this work.

The lowest lying black line in the central part of the spectrum ($F_z = -10$ kV/cm) is connected with a *united* trion state in the results for both Hamiltonians (see diagrams). On the left side of that point, the level behavior is also the same: an electron tunnels to the bottom dot leading to a complete *disruption* of the trion state. On the right side of the central part, the behavior of the black line with increasing F_z is connected to the hole tunneling and differs depending on the model. Like earlier for the strong coupling case, for closer investigation, the singlet-singlet and final hole states energy difference was calculated and the tunneling intervals determined (Fig. 6). The obtained intervals have been also marked on relevant fragments of the spectrum (Fig. 7). In the KL computation for $F_z \in (-0.7,2.1)$ kV/cm, one of the holes of the trion state tunnels to the bottom dot and then for $F_z \in (3.3,5.5)$ kV/cm the final hole in the ground-state tunnels to the bottom dot (the *united* type level continues as the blue and then brown line visible in Fig. 5, like described in the previous paragraph). The result is a large (over 2 meV) rapid descent of the black energy level. This tunneling sequence is the same as in the strong coupling case and leads to the formation of a distinct conformation of levels and their anticrossings, which is known as the X pattern [22]. Next, in a field interval $F_z \in (5.5,34.5)$ kV/cm, the level corresponds to the *dissociated* trion case. Afterward, for $F_z \in (34.5,37.2)$ kV/cm, the second hole part in the trion state tunnels to the bottom dot resulting in a *disruption* of the trion state. In the separated-bands model for $F_z \in (4.5,5.6)$ kV/cm, a hole in the initial state tunnels to the bottom dot and, simultaneously, for $F_z \in (4.3,5.2)$ kV/cm, the final hole in the ground-state tunnels to the bottom dot.

One should note (i) the reversed tunneling sequence with respect to the results of the KL model for a 7.1-nm barrier and for both models in the strong coupling case and (ii) the fact that the tunneling intervals largely overlap (also in contrary to previously presented results). Those changes in the tunneling process are connected to another shape of the spectrum: a relatively small but rapid increase in energy. The sole reversed order of the tunneling of the initial and final state holes would cause an appearance of a X pattern reversed in energy with respect to the KL model. This is because both holes tunnel in the same way, but the energy of the recombination level is equal to the energy of the initial trion state minus the energy of the final hole state. Thus the impacts of both tunneling processes on the dipole moment are of opposite signs. However, the overlap of the mentioned intervals destroys the X pattern. As the recombination level gets two dipole moment shifts of opposing signs and similar magnitude nearly simultaneously (in terms of F_z), the resulting overall energy shift is relatively small.

Finally, for $F_z \in (29.2,30.4)$ kV/cm, the second hole tunnels to the bottom dot and *disrupts* the trion state. The difference between the qualitatively very distinct phenomena of the large rapid decrease and small rapid increase in energy is effectively an effect of the blueshift/redshift change of the *united* trion level (as the *dissociated* trion level energy is always convergent to the exciton level energy).

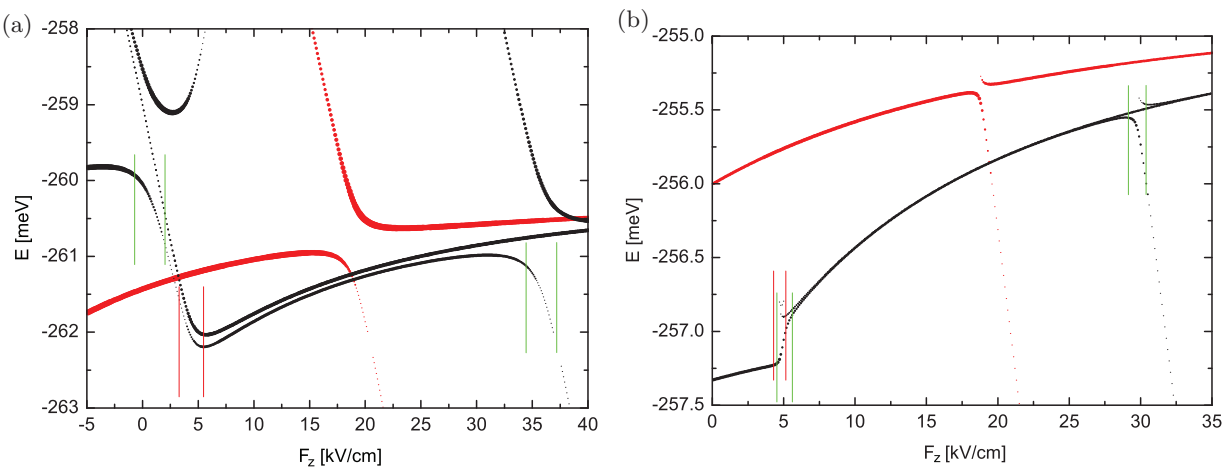

FIG. 7. (Color online) Fragments of corresponding spectra from Fig. 5 with tunneling intervals from Fig. 6 marked by vertical lines: green for trion state hole, red for final state hole.

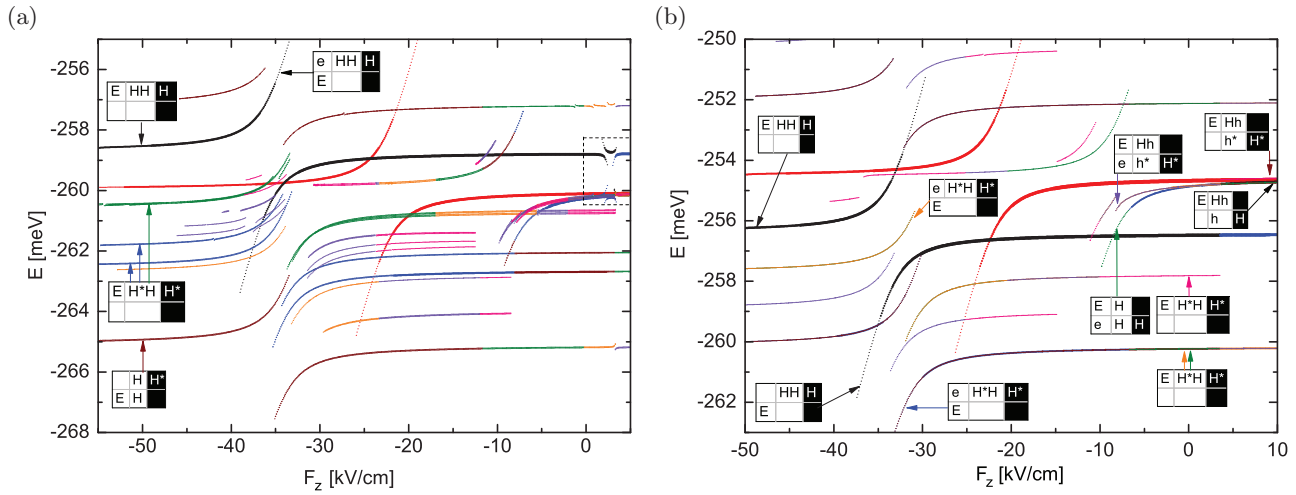

FIG. 8. (Color online) Same as Fig. 2 only for interdot barrier of 10.1 nm. Blue color is for a trion recombination to a hole first excited state and the other colors are for successive excited final hole states. The dotted line indicates the region presented in Fig. 10(a).

The process of a steplike trion dissociation similar to the one described above for Fig. 5(a) is visible in Fig. 1(a) of Ref. [18]. The rapidly descending positive trion recombination level crosses the neutral exciton line before the latter is involved in an anticrossing corresponding to the exciton dissociation.

The recombination probability reversal is not present for 7.1 nm barrier thickness, due to the weaker tunnel coupling with respect to 4.1 nm. There is no region where the particle distribution between the dots is approximately equal so that the recombination probability would be governed by the bonding/antibonding character of the states.

E. Asymmetric dots, weak interdot coupling

The results for a barrier thickness of 10.1 nm are presented in Fig. 8. The series of wide anticrossings that result from the electron tunneling are the main feature of the central part of the spectra (like in Fig. 5). Both the levels connected to the *dissociated* and those connected to the *united* trion states are visible. *United limit levels* have energy of circa −259 meV for both $F_z = -55$ kV/cm (black line) and $F_z = 5$ kV/cm (black and then blue line) in the case of the KL Hamiltonian and −256 meV for both $F_z = -50$ and 10 kV/cm in the case of the separated-band Hamiltonian. The *dissociated limit levels* are present as the blue and then black lines with energies convergent to the neutral exciton. Numerous other states with nearly zero dipole moment appear in Fig. 8 for the KL and separated-bands case. Those levels are similar to either the united or the dissociated trion levels with the difference that one of the holes in the trion state is in-plane excited (see diagrams, the excitation is marked with an asterisk) and the final hole state is an in-plane excited state (hence the various line colors).

For closer investigation of the trion dissociation process, the singlet-singlet and final hole states energy difference was calculated and the tunneling intervals determined (see Fig. 9). The obtained intervals have been also marked on fragments of relevant spectra (see Fig. 10).

The process of 2-step trion dissociation for the KL Hamiltonian in the system of two dots with 10.1-nm barrier is the same as for the barrier thickness of 7.1 nm. The "ground black line" corresponds to the united trion state in the interval of about $F_z \in (-30, 1.67)$ kV/cm. In the field intensity scope of (1.67, 2.64) kV/cm, a trion hole tunneling to the other dot occurs. For $F_z \in (2.91, 3.70)$ kV/cm, the final hole in the ground-state tunnels to the bottom dot. The step of complete trion disruption is not visible as it lies beyond the scope of the figure ($F_z >$ 5 kV/cm). The X pattern that is located at the right end of this interval is analogous to the one in Fig. 5(a). The black line continues after a rigid drop with energy slightly smaller than the neutral exciton line energy [clearly visible in Fig. 10(a)].

This kind of X pattern for a positive trion has been observed experimentally in Ref. [19] [see Fig. 1(b), the frame with X+ symbol; keep in mind the reversed direction of electric field and neglect the electron-hole exchange energy in our work].

In the case of the separated-bands Hamiltonian for barrier thickness 10.1 nm the black line appears to have a jump discontinuity in the full-scope picture, Fig. 8(b), but is in fact continuous as can be seen in the more detailed Figs. 10(b) and 10(c). The character of the "ground black line" for 10.1 nm is somewhat similar to the 7.1 nm case. The hole tunneling sequence is also reversed with respect to KL model, as the final hole and trion hole tunneling intervals are (3.566, 3.599) and (4.957, 5.023) kV/cm, respectively. The difference is that in the weak-coupling case the two hole tunneling intervals are completely separated.

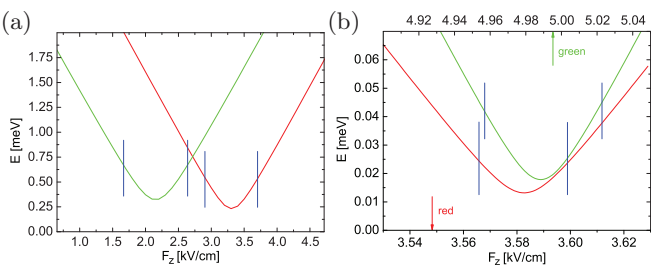

FIG. 9. (Color online) Same as Fig. 3 only for interdot barrier of 10.1 nm. The top scale in (b) is for the green line and the bottom scale is for the red line.

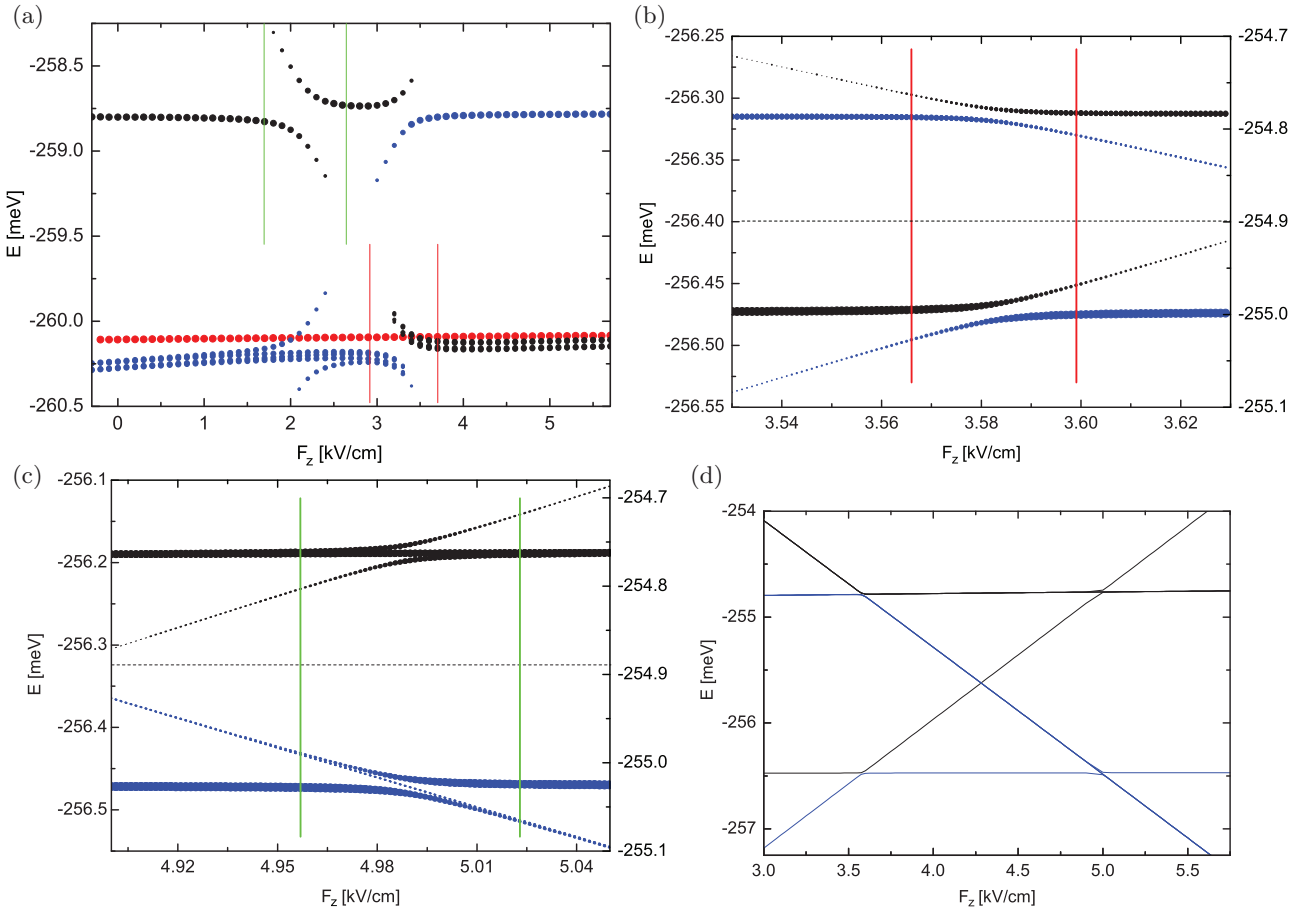

FIG. 10. (Color online) (a)–(c) Fragments of the corresponding spectra from Fig. 8 with tunneling intervals from Fig. 9 marked by vertical lines: green for a trion state hole, red for a final state hole. (a) is for KL, (b) and (c) are for separated-bands models. Left and right energy scales in (b) and (c) describe bottom and top halves of the relevant picture, respectively. The linewidth is proportional to the square root of the recombination probability. (d) A fragment of the spectrum in Fig. 8(b) without recombination probabilities.

The visibility of the X pattern depends on the relative position of the tunneling intervals. The nonhorizontal levels (with high dipole moment) acquire visibility only near relevant anticrossings. If the anticrossings include only small F_z intervals and are completely separated [like in Fig. 8(b) case] then the X pattern is absent from the recombination spectrum as the relevant recombinations are forbidden. To illustrate this more clearly, the energy (and not the recombination probability) of the relevant levels is presented in Fig. 10(d). The black line shifts downward in energy with increasing F_z and the blue line shifts upward in the KL model results [Fig. 10(a)]. The results of unmixed HH/LH subbands exhibit reversed pattern [Fig. 10(a)]. This is a consequence of the reversed hole tunneling sequence (Fig. 9) and was already discussed in the previous section. Apart of that the X patterns are similar [compare Figs. 10(a) and 10(d)]. It should be noted that the substantially larger tunneling intervals widths in the KL model are a consequence of the mixing of the LH components into the HH-mainly states. The light holes are significantly weakly localized in the dots and thus have greater tunnel coupling and this causes also increase in tunneling couplings of the relevant states in the KL model.

F. Symmetric dot pair

Let us now focus on a special case of the system of two dots of identical size. We assume the height of both the bottom and the top dot to be 2.0 nm in this case. The calculated spectra for the symmetric dot system are presented in Figs. 11, 12, and 13 for various barrier thickness; (a) shows the results of the KL model and (b) of the separated bands.

The 4.1-nm and 7.1-nm results have similar characteristics. At $F_z = 0$, four trion recombination levels attain energy extrema and their initial states are singlet, triplet, singlet, and singlet in the order of increasing energy. In the absence of electric field, they are grouped in two pairs; levels in a single pair have nearly the same particle densities and differ in the expected parity with respect to reverting the z axis (the bonding/antibonding character). The difference between the pairs is the excitation of the trion state in the upper pair as both the charge density distribution and the light-hole component (in the KL model) are nearly the same (7.3% lower pair, 6.5% upper pair). More specifically, this is a mainly hole axial type excitation.

For a symmetric system, separated-bands and noninteracting particles, in the Hamiltonian eigenstate, the parity with

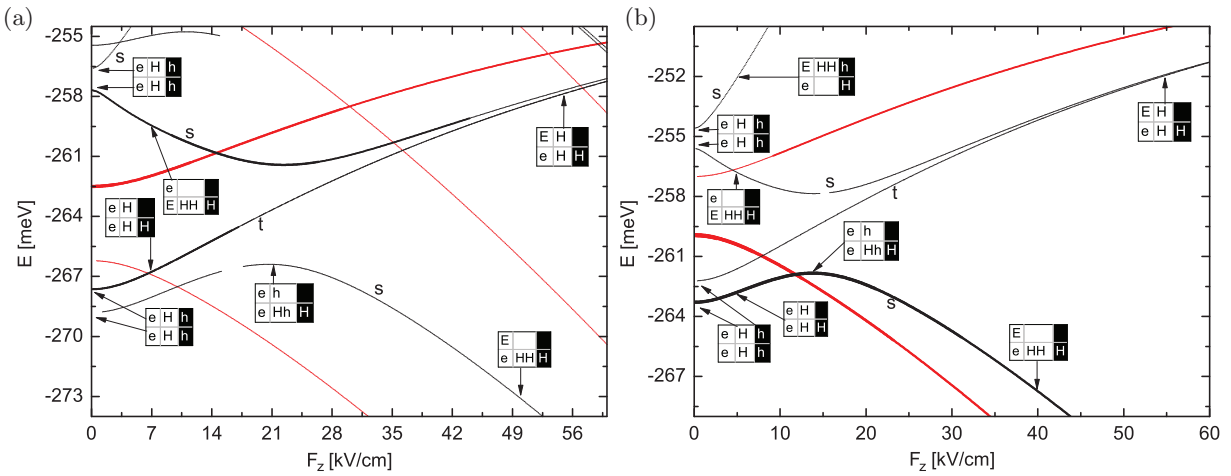

FIG. 11. (Color online) Energy spectrum and recombination probabilities (marked as linewidth) for positive trion (black) and exciton (red lines) vs electric field intensity parallel to z axis. The case of symmetric dots with barrier width $D = 4.1$ nm. (a) For KL Hamiltonian and (b) for unmixed HH and LH bands Hamiltonian. Red color indicates the exciton recombination, black is for trion recombination to hole ground state. Particle localization diagrams are described in the text. "S" denotes a singlet state, "t" denotes a triplet state.

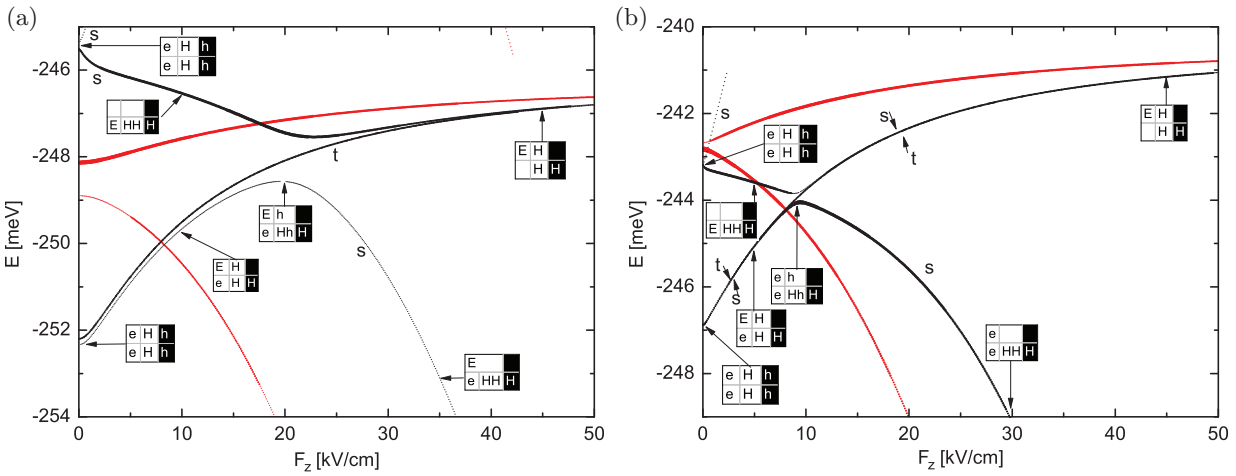

FIG. 12. (Color online) Same as Fig. 11 only for interdot barrier of 7.1 nm.

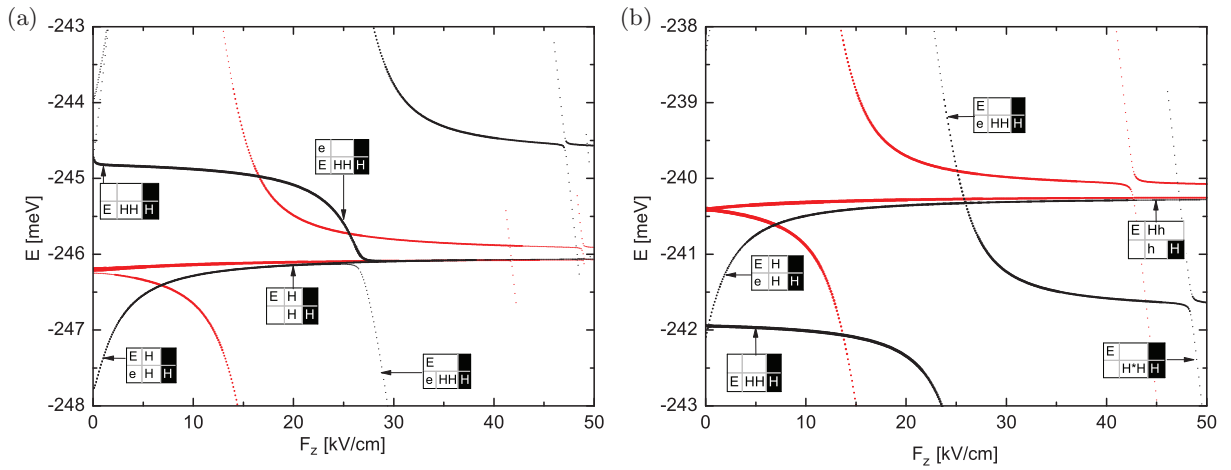

FIG. 13. (Color online) Same as Fig. 11 only for interdot barrier of 10.1 nm.

respect of reversing the z axis is always defined. This is the case of the final hole in the separated-bands Hamiltonian and for each of the four components of the KL wave function. However, the parity of the whole KL eigenstate is not defined nor is the parity of the hole trion part. Hence the states will be described in terms of their dominating bonding character.

The probability maximum/minimum reversal is visible in all symmetric systems spectra. However, as the tunnel coupling decreases in strength, the scope of F_z where reversal phenomena appear also decreases and the effects become significantly less pronounced. The expected value of the parity of the final hole ground state is -0.89 in the KL case and 1.00 in the separated-bands case (defined parity). The electron has a bonding character in low lying states as discussed before. The "bonding/antibonding character description" for the trion states is $(+,(+,+),+)$, $(+,(+,-),+)$, $(+,(+,-),+)$, $(+,(-,-),+)$ in the case of Figs. 11(b) and 12(b) and $(+,(-,-),-)$, $(+,(+,-),-)$, $(+,(+,-),-)$, $(+,(+,+),-)$ in the case of Figs. 11(a) and 12(a) in ascending energy order. An analysis analogous to the one concerning the bonding character in the asymmetric system can be made leading to the same conclusion about the reason of the reversal of recombination probabilities.

The first and the second singlet-state levels form an anticrossing for $F_z = 21$, 14, 20, and 9 kV/cm in the cases of KL 4.1 nm, separated-bands 4.1-nm, KL 7.1-nm, and separated-bands 7.1-nm systems, respectively. The lower triplet-state level runs straight through this anticrossing as the singlet and triplet trion states do not mix with each other in the presence of electric field. This anticrossing originates from the process of the trion ground-state dissociation (one hole part along with the electron part tunnels to the other dot). The process is continuous as in the case of Fig. 2 rather than having rapid step character like in Figs. 5 or 8.

The low dipole moment strong field *limit levels* have energy of about -257 meV for $F_z = 60$ kV/cm in Fig. 11(a), -251 meV for $F_z = 60$ kV/cm in Fig. 11(b), -247 meV for $F_z = 50$ kV/cm in Fig. 12(a), and -241 for $F_z = 50$ kV/cm in Fig. 12(b). These states are of *dissociated* trion type. The *united limit levels* are not present in the energy range of Fig. 12 and do not play a role in the dissociation process of the trion.

The situation is different in the case of the largest barrier thickness (Fig. 13). Both types of the *limit levels* are visible with the blueshift/redshift change of the *united limit levels* between the models. The shift type determines the ground-level behavior and the type of the trion dissociation. First, in the KL case, the line stabilizes in energy; the level becomes *dissociated* [$F_z \in (10,20)$ kV/cm]. Then it is completely *disrupted* by the energy hole tunneling (the small anticrossing at about $F_z = 27$ kV/cm). In the separated-bands case, it is nearly stabilized almost from $F_z = 0$ as the *united* trion type level and then trion is *disrupted* by high-energy electron tunneling [large anticrossing at $F_z \in (20,30)$ kV/cm].

G. Comparison with negative trion

The obtained results can be compared to the ones of previous work [33] in order to isolate the positive and negative trion spectra characteristics. In the case of asymmetric dots with 4.1-nm barrier width (Fig. 2 and Figs. 2, 5(a), and 6(a) in Ref. [33]), the main difference is that the black *limit level* is connected to the *united* negative trion, while it corresponds to the *dissociated* state in the case of positive trion. The origin of this is the difference between electron-electron and hole-hole interaction strengths in relation to the difference between the effective masses of the two particles. The negative trion recombination spectrum in the system with barrier thickness of 10.1 nm (see Figs. 3, 5(b), and 6(b) in Ref. [33]) is strongly different than the relevant positive trion one (Fig. 8). In the former, the gradual trion dissociation process is pronounced while in the latter it occurs but it is weakly recognizable. Hence the comparison to the positive trion case system with barrier width 7.1 nm is more justified. The negative trion state in the first "stable region" (i.e., the interval for which the level has a low dipole moment just right from the electron-tunneling anticrossing; $F_z \in (-27, -18)$ kV/cm in Figs. 3(a) and 3(b) Ref. [33]) is *dissociated* and the positive trion in that region is *united* [$F_z \in (-20, -5)$ kV/cm in Fig. 5(a), $F_z \in (-10,5)$ kV/cm in Fig. 5(b)]. With increasing value of the electric field the negative trion switches to the *united* trion state ($F_z \in (-5,30)$ in Fig. 3(a) and 3(b) Ref. [33]), while the positive trion *dissociates* [$F_z \in (10,30)$ kV/cm in Fig. 5(a), $F_z \in (10,25)$ kV/cm in Fig. 5(b)] before the final *disruption*. In conclusion, differently charged trions have an opposite dissociation mechanism as a reaction to applied external electric field. This is also directly connected to the reversed roles that the field limit of mentioned levels have in these two cases: the black *limit levels* on the left pictures edges denote the *dissociated* negative trion, as opposed to indicating *united* positive trion (both Figs. 5 and 8). The blueshift/redshift change in those levels in reference to the exciton *limit level* is absent for a negative trion as it happens only with *united* trion type *limit levels*.

IV. DISCUSSION

Note that the X pattern discussed in Secs. III D and III E was also obtained by the heavy-hole approximation and frozen lateral degree of freedom in Ref. [22] (compare the dissociation pattern of Fig. 5(a) with Fig. 6(b) in the mentioned work). Our calculations with the separated-bands Hamiltonian for holes do not yield this experimentally observed pattern in any coupling regime. This is due to three reasons. Firstly, in the strong coupling regime, X patterns simply do not occur in either the KL or unmixed-bands Hamiltonians due to a completely different arrangement of the recombination levels. Secondly, for a barrier width of 7.1 nm, the tunneling intervals of the initial state hole and the final state hole overlap. Thirdly, the tunneling intervals of the initial state hole and the final state hole are completely separated for a barrier width of 7.1 nm. The occurrence of the X pattern with the separated-bands Hamiltonian would require the hole tunneling intervals to be adjacent but not considerably overlapping. This could be managed by choosing appropriate parameters of the system and by that restoring the X pattern into a recombination spectrum.

V. SUMMARY AND CONCLUSIONS

In this work, we have calculated and described the recombination spectra of positive trions in an artificial molecule consisting of two vertically coupled quantum dots in an

external electric field. Both a realistic asymmetric case and a theoretically interesting symmetric system were studied. Moreover, we described qualitative changes in the trion dissociation process depending on the model type and the barrier width between the dots.

We found that the most remarkable difference between the KL and unmixed-bands Hamiltonians results in the strong-coupling regime (Sec. III A) is the reversal of the maximum and the minimum of recombination probability. For the KL model, the ground level has a *minimum* of the recombination probability in the vicinity of $F_z = 0$ and the first excited level has *maximal* recombination probability in the same region. For the separated-bands model, the pattern is reversed. We pointed to the mixing of light- and heavy-hole bands that leads to the formation of an antibonding hole ground state as a reason for this phenomenon. For medium and weak interdot coupling regimes (Secs. III D and III E), the trion *united* level of the lowest energy in the strong F_z limit is *blueshifted* in the case of the KL model and *redshifted* in the case of the unmixed-bands model. We have also indicated that in these coupling regimes the present calculation with the KL Hamiltonian reproduces the experimentally observed X pattern of Ref. [19]. We have demonstrated that for the same parameters the single-band approximation of the hole does not reproduce the experimental features and yields instead qualitatively and quantitatively different results. In Sec. III G, we found that the recombination probability maximum/minimum reversal between the KL and separated-bands models in the positive trion spectra is present for both positive and negative trions. However, significant differences between the negative and the positive trion dissociation processes have been found: (i) the redshift/blueshift change between the models in the united trion type *limit levels* and (ii) the change of trion dissociation process type. The qualitative differences between the positive and negative trion spectra described above are quite significant and may be helpful in the process of experimental lines recognition.

ACKNOWLEDGMENTS

This work was supported by the Polish Ministry of Science and Higher Education, by the EU Human Capital Operation Program, Project No. POKL.04.0101-00-434/08-00, and by National Research Centre according to decision DEC-2012/07/N/ST3/03161. This research was supported in part by PL-Grid Infrastructure.

[1] G. S. Solomon, J. A. Trezza, A. F. Marshall, and J. S. Harris, Jr., Phys. Rev. Lett. **76**, 952 (1996).
[2] N. N. Ledentsov, V. A. Shchukin, M. Grundmann, N. Kirstaedter, J. Bohrer, O. Schmidt, D. Bimberg, V. M. Ustinov, A. Y. Egorov, A. E. Zhukov, P. S. Kopev, S. V. Zaitsev, N. Y. Gordeev, Z. I. Alferov, A. I. Borovkov, A. O. Kosogov, S. S. Ruvimov, P. Werner, U. Gosele, and J. Heydenreich, Phys. Rev. B **54**, 8743 (1996).
[3] S. Fafard, M. Spanner, J. P. McCaffrey, and Z. R. Wasilewski, Appl. Phys. Lett. **76**, 2268 (2000).
[4] D. Kim and D. Gammon, Solid State Commun. **149**, 1427 (2009).
[5] A. Greilich, S. C. Badescu, D. Kim, A. S. Bracker, and D. Gammon, Phys. Rev. Lett. **110**, 117402 (2013).
[6] A. Greilich, S. G. Carter, D. Kim, A. S. Bracker, and D. Gammon, Nat. Photon. **5**, 702 (2011).
[7] A. I. Yakimov, A. A. Bloshkin, and A. V. Dvurechenskii, Phys. Rev. B **81**, 115434 (2010).
[8] S. E. Economou, J. I. Climente, A. Badolato, A. S. Bracker, D. Gammon, and M. F. Doty, Phys. Rev. B **86**, 085319 (2012).
[9] K. De Greve, P. L. McMahon, D. Press, T. D. Ladd, D. Bisping, C. Schneider, M. Kamp, L. Worschech, S. Höfling, A. Forchel, and Y. Yamamoto, Nat. Phys. **7**, 872 (2011).
[10] T. M. Godden, J. H. Quilter, A. J. Ramsay, Yanwen Wu, P. Brereton, S. J. Boyle, I. J. Luxmoore, J. Puebla-Nunez, A. M. Fox, and M. S. Skolnick, Phys. Rev. Lett. **108**, 017402 (2012).
[11] J. I. Climente, M. Korkusiński, G. Goldoni, and P. Hawrylak, Phys. Rev. B **78**, 115323 (2008).
[12] M. F. Doty, J. I. Climente, M. Korkusiński, M. Scheibner, A. S. Bracker, P. Hawrylak, and D. Gammon, Phys. Rev. Lett. **102**, 047401 (2009).
[13] J. I. Climente, Appl. Phys. Lett. **93**, 223109 (2008).
[14] T. Chwiej and B. Szafran, Phys. Rev. B **81**, 075302 (2010).
[15] D. Reuter, P. Kailuweit, A. D. Wieck, U. Zeitler, O. Wibbelhoff, C. Meier, A. Lorke, and J. C. Maan, Phys. Rev. Lett. **94**, 026808 (2005).
[16] Y. Komijani, M. Csontos, T. Ihn, K. Ensslin, D. Reuter, and A. D. Wieck, Europhys. Lett. **84**, 57004 (2008).
[17] M. F. Doty, M. Scheibner, A. S. Bracker, I. V. Ponomarev, T. L. Reinecke, and D. Gammon, Phys. Rev. B **78**, 115316 (2008).
[18] M. F. Doty, M. Scheibner, I. V. Ponomarev, E. A. Stinaff, A. S. Bracker, V. L. Korenev, T. L. Reinecke, and D. Gammon, Phys. Rev. Lett. **97**, 197202 (2006).
[19] M. Scheibner, M. F. Doty, I. V. Ponomarev, A. S. Bracker, E. A. Stinaff, V. L. Korenev, T. L. Reinecke, and D. Gammon, Phys. Rev. B **75**, 245318 (2007).
[20] X. R. Zhou, J. H. Lee, G. J. Salamo, M. Royo, J. I. Climente, and M. F. Doty, Phys. Rev. B **87**, 125309 (2013).
[21] J. I. Climente, A. Bertoni, and G. Goldoni, Phys. Rev. B **78**, 155316 (2008).
[22] M. H. Degani and M. Z. Maialle, Phys. Rev. B **75**, 115322 (2007).
[23] S. L. Chuang, *Physics of Photonic Devices*, 2nd ed. (Wiley, New York, 2009), pp. 165–166.
[24] I. Vurgaftman, J. R. Meyer, and L. R. Ram-Mohan, J. Appl. Phys. **89**, 5815 (2001).
[25] M. Stopa and C. M. Marcus, Nano Lett. **8**, 1778 (2008).
[26] G. Bastard, *Wave Mechanics Applied to Semiconductor Heterostructures*, 1st ed. (Halsted Press, New York, 1988).
[27] V. Jovanov, S. Kapfinger, M. Bichler, G. Abstreiter, and J. J. Finley, Phys. Rev. B **84**, 235321 (2011).
[28] The exact way of calculating photon-related relaxation probabilities, trion dissipation probabilities, and other nonradiative processes that lead to a decrease in the observed photoluminescence signal is outside the scope of this work. A complete neglect of these processes gives spectra with hundreds of optically active

lines. These spectra are completely illegible due to sheer number of lines and they obviously have nothing in common with experimental data. In Ref. [33], we set the value of $E_r = 34$ meV to best match our results with the experimental ones. As the Boltzmann-like factor is a very rough method of taking into account many complex mechanisms, the value of E_r is only a fit parameter and has no physical meaning. We decided to use the same value in this work to enable a direct comparison between the results for the positive and negative trions.

[29] In some of the pictures, only a limited set of final states has been taken into consideration. This is motivated by the simplicity of interpretation and by the fact that showing too many lines would have made the main results of our work indistinct. However, in the other figures, more colors are presented (more final hole states taken into account) as it is necessary for understanding the presented processes.

[30] The energy difference between the levels involved in an anticrossing is a parabola near the minimal energy difference. Sufficiently far from that point, the difference should be nearly linear as a result of subtraction of two nearly linear functions. Hence we take points where $\frac{|f'|}{f''} = \alpha$ as the estimates of ends of a tunneling interval, where f is the relevant energy difference, with $\alpha = 2$. An exception is the weak-coupling separated-bands case, where $\alpha = 0.2$ is taken because of the completely different energy scale of that case.

[31] Our analysis of obtained results uses the presented naming convention. Also, the trion state is a mixture of basis states of different bonding characters of the hole part in the meaning described above. We adopt a simplifying naming convention that assigns "bonding" or "antibonding" to the hole part in the trion state on the basis of the dominant components of the trion eigenstate. In the case that we describe one hole in the trion as bonding and the other as antibonding, we in fact describe occupied orbitals.

[32] Some of the lines in Figs. 5 and 8 are discontinued. This is an effect of the fact that we have presented levels resulting from recombination only to a finite set of the final hole states.

[33] W. J. Pasek and B. Szafran, Phys. Rev. B **85**, 085301 (2012).